Robot Bed-Making: Deep Transfer Learning Using Depth Sensing of Deformable Fabric

Daniel Seita*,1, Nawid Jamali*,3, Michael Laskey*,1, Ron Berenstein[1], Ajay Kumar Tanwani[1,2], Prakash Baskaran[3], Soshi Iba[3], John Canny[1], Ken Goldberg[1,2]

***Abstract*— Bed-making is a common task well-suited for home robots since it is tolerant to error and not time-critical. Bed-making can also be difficult for senior citizens and those with limited mobility due to the bending and reaching movements required. Autonomous bed-making combines multiple challenges in robotics: perception in unstructured environments, deformable object manipulation, transfer learning, and sequential decision making. We formalize the bed-making problem as one of maximizing surface coverage with a blanket, and explore algorithmic approaches that use deep learning on depth images to be invariant to the color and pattern of the blankets. We train two networks: one to identify a corner of the blanket and another to determine when to transition to the other side of the bed. Using the first network, the robot grasps at its estimate of the blanket corner and then pulls it to the appropriate corner of the bed frame. The second network estimates if the robot has sufficiently covered one side and can transition to the other, or if it should attempt another grasp from the same side. We evaluate with two robots, the Toyota HSR and the Fetch, and three blankets. Using 2018 and 654 depth images for training the grasp and transition networks respectively, experiments with a quarter-scale twin bed achieve an average of 91.7% blanket coverage, nearly matching human supervisors with 95.0% coverage. Data is available at `https://sites.google.com/view/bed-make`.**

I. Introduction

A common home task is bed-making [4], which is rarely enjoyed and can be physically challenging due to bending and leaning movements. Surveys of older adults in the United States [9], [3], suggest that they are willing to have a robot assistant in their homes, particularly for physically demanding tasks. Home robotics offers the potential to provide treatment and care to senior citizens and people with limited dexterity [5], [10]. Bed-making is a task well-suited for home robots since it is tolerant to error and not time-critical.

We formulate bed making as an optimization problem where a robot grasps and then pulls at blanket corners to maximize coverage over the bed frame. We focus on cases when a blanket is fixed in two corners (called "mitred" in hospitals [4], [32], [15]). The focus on corners as grasping points has also been central to robotic manipulation of towels [24] and laundry [27].

Detecting a suitable grasp point is challenging because the blanket may be highly wrinkled. In addition, due to sensor noise and imprecision in actuation, a grasp and pull on the blanket may fail to adequately cover the bed frame.

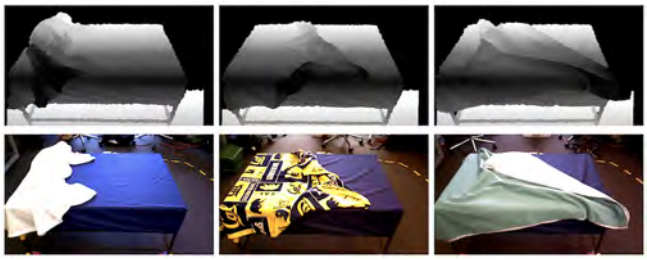

Fig. 1: Example pairs of depth (top) and RGB (bottom) images from three bed-making states of increasing coverage as seen through a robot's head camera sensors. Our system uses depth images to train policies and generalizes to white, Cal-patterned, and teal blankets.

We learn two policies parameterized by deep convolutional neural networks: a *grasp* policy and a *transition* policy, both of which receive as input a depth image of the bed from head camera sensors. The grasp policy decides the (x, y) pixel location of where to grab the blanket. The transition policy decides if the blanket has sufficiently covered the frame, and thus whether or not to try pulling the blanket again. Using depth images allows both policies to generalize to blankets with different colors and patterns, as shown in Figure 1.

We collect data from humans supervising the bed-making task (see Section IV-C), and train both policies using deep learning to map images to actions. To reduce data collection and training time, we leverage a pre-trained RGB object detection network, YOLO [34]. The policies are deployed on two robots: the Toyota Human Support Robot (HSR) [13] and the Fetch Robot [42], which both have a mobile base and one arm equipped with a two-jaw gripper.

Results suggest that a neural network policy trained with 2018 depth images (of the white blanket) can achieve 91.7% coverage, nearly matching performance of 95.0% when a human selects grasp points. The policy also transfers to Cal-patterned and teal blankets with 92.5% coverage, suggesting robustness to varying blanket configurations and patterns.

This paper contributes: 1) a formalization of the bed-making problem in terms of maximizing coverage, 2) deep learning algorithms based on depth images to estimate grasp points, making the system invariant to colors and patterns, 3) a procedure for collecting training data using RGB and depth images to autonomously label grasp points, reducing human effort, 4) experimental data with a quarter-scale twin bed, two mobile robots, and three blankets.

This paper is a greatly expanded and revised version of an earlier unpublished preprint [20].

* These authors contributed equally.
[1] Department of Electrical Engineering and Computer Sciences; {laskeymd,seita,ron.berenstein,ajay.tanwani,canny,goldberg}@berkeley.edu
[2] Department of Industrial Engineering and Operations Research
[1−2] AUTOLAB at the University of California, Berkeley, USA
[3] Honda Research Institute, USA; {njamali,pbaskaran,siba}@honda-ri.com

II. Related Work

A. Assistive and Home Robotics

Recent research on assistive and home robotics includes [37], which designed a robotic bed equipped with pressure sensors to anticipate the pose of a patient. Another robotic system was developed in [28] which could lift patients in and out of bed. Other recent capabilities include bed wipes [16], and assisted dressing, feeding, and navigation [43], [7], [31], [41]. Such work focuses on different aspects of home robotics and is orthogonal to our contribution.

In the commercial setting, some "smart beds" such as the Ohea [30] have the ability to make themselves, but these systems are proprietary and not widely used, whereas a mobile robot can be deployed to make different beds.

There has also been recent interest in using machine learning to train home robots [12]. While [12] avoided depth data due to cost, we utilize higher-quality robots and generalize our preliminary bed-making task [20] by using depth images available in our robot's sensors, in a manner similar to recent data-driven grasping methods [23]. To our knowledge, this is the first paper on robot bed-making.

B. Manipulation of Deformable Objects

Manipulation of cloth has been explored in a variety of contexts, such as folding of laundry [27], [39]. For instance, [24] used an algorithm based on identifying and tensioning corners to enable a home robot to fold laundry, and [6] used a Hidden Markov Model and deformable object simulator to bring clothing into an arbitrary position. Additional techniques for cloth manipulation range from tracking using point clouds [36], learning from demonstrations [2], [21], and using deep reinforcement learning in simulation [26].

In the surgical setting, the task of cutting tissue is similar to the task of cutting cloth. For example, [29] examined cutting a circle out of surgical gauze via leveraging expert demonstrations, but the approach was highly hand-tuned and suffered from imprecision of the optimal grasp points on cloth. A more robust tensioning policy was developed in simulation using deep reinforcement learning [40]. Such techniques, however, rely on having an accurate simulator, which is not generally available for deformable objects.

C. Behavior Cloning and Deep Learning

Supervised learning, in the form of behavior cloning, is a popular imitation learning technique that has been applied to a wide variety of tasks such as self-driving cars [33], quadcopter flight [35], grasping in clutter [19], and virtual reality teleoperation [44]; see [1] for a survey. Similarly, to learn robust grasp and transition policies that generalize across blanket configurations, we use deep convolutional neural networks [18], [11]. To collect data, we use a human to manually perform the task (not through teleoperation) by repeatedly pulling a blanket and collecting images.

III. Problem Statement

A. Assumptions and Definitions

Robot. We assume a mobile robot with an arm, an end-effector, and color and depth cameras. We assume it is able to reach at least anywhere on the half of the bed closest to its position. We additionally assume that blanket corners are reachable and visible from head sensor cameras.

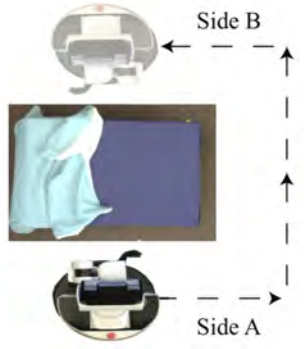

Fig. 2: A top-down view of the setup for one rollout. A robot (in this case, the HSR) starts on Side A and executes the grasp and transition policies for that side. Then, it traverses to Side B to mirror the scene over the y-axis, and again deploys the policies. It terminates after finishing Side B.

Bed. A bed is composed of a *frame* and a *blanket*. The frame is a rigid rectangular 3D structure with dimensions $W_F \times H_F \times L_F$. The physical space occupied by the *top surface* of the frame is a 2D xy-plane. The blanket is deformable cloth and can be characterized with an occupancy function $\xi : \mathbb{R}^3 \rightarrow \{0, 1\}$ to determine if a 3D point is part of the blanket or not. Here, ξ represents the blanket configuration; let Ξ be the space of all possible configurations. As the bed frame is fixed and known, ξ is sufficient to express the state.

We additionally define the function $f_\xi(x, y)$ to be the height of the highest point of blanket ξ at location (x, y) of the top surface plane, or 0 if the (x, y) point is uncovered. This naturally leads to the *top envelope* E_ξ of the blanket to be the set of visible points of the blanket from a top-down view:

$$E_\xi = \left\{ (x, y, f_\xi(x, y)) : f_\xi(x, y) > 0, x \in \tilde{X}, y \in \tilde{Y} \right\} \quad (1)$$

where $\tilde{X} = [x_1, x_2]$ and $\tilde{Y} = [y_1, y_2]$ represent appropriate coordinate ranges over the top surface plane.

B. Objective

We benchmark the bed-making objective in terms of surface coverage of the blanket ξ over the top surface of the bed. Denoting the function $c : \xi \rightarrow [0, 1]$ which computes the percentage of the top surface covered by the blanket, our objective is to maximize the coverage:

$$\underset{\xi \in \Xi}{\text{maximize}} \;\; c(\xi). \quad (2)$$

Given a blanket configuration ξ, the problem of finding an optimal grasp point can be formulated as finding the point $(x, y, f_\xi(x, y)) \in E_\xi$ such that coverage is maximized when the neighborhood of points about it on E_ξ are gripped and pulled to the uncovered corner nearest to the robot.

IV. Setup and Methodology

Our proposed algorithm involves a robot pulling at a corner of the blanket to the side nearest to it (using multiple attempts if needed), and then moving to the other side of the bed and repeating the process. See Figure 2 for one rollout.

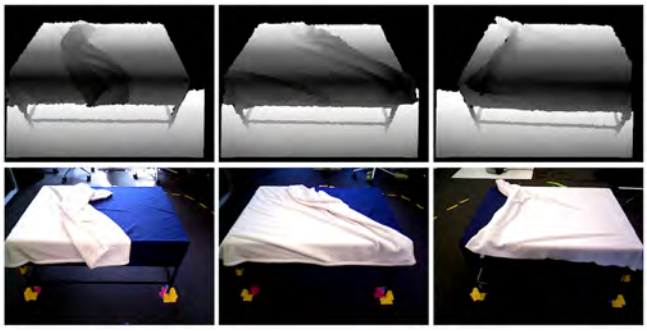

Fig. 3: Examples of images for training the transition network. First column: an unsuccessful case. Second column: a successful case. Third column: (on the other side of the bed) a borderline case which could be either depending on a human's preferences; we labeled this as a failure. The transition network must also operate when the robot is on the second side of the bed (e.g., as in the third column). In addition to borderline cases, the task can be challenging due to differences in viewpoints and varying human predilections.

A. The Robots and The Bed

We use two mobile robots, the HSR and the Fetch, to evaluate the generality of this approach. The HSR [13] has an omnidirectional base [22] to allow joint planning with its 4 DoF base and 3 DoF arm. The Fetch [42] has a longer 7 DoF arm and a differential drive base. Both robots have head camera sensors which can return depth and RGB images.

We use a quarter-scale bed frame with dimensions $W_F = 67$ cm, $H_F = 45$ cm, and $L_F = 91$ cm. The bed consists of one blanket with size slightly larger than the frame so that a human could comfortably cover it. One end of the blanket is fixed to one of the shorter sides of the bed frame to simulate two corners being tucked under a mattress.

B. Grasp and Transition Policies

To maximize bed frame coverage (Equation 2), the robot learns to grasp at one of two corners of the blanket,[1] and then pulls it towards the appropriate corner of the bed frame. In addition, to be robust to failure, we also propose that the robot learn whether to retry pulling the blanket or to transition to the other side of the bed. These involve learning policies that act on *observations* $\mathbf{o}_t \in \mathbb{R}^{640\times480\times3}$ at time t, which are depth images from the robot's head camera sensors.

We define a *grasp policy* $\pi_{\theta_G} : \mathbb{R}^{640\times480\times3} \rightarrow \mathbb{R}^2$ parameterized by θ_G as a mapping from $\mathbf{o}_t$ to a pixel position $\mathbf{u}_t^{(G)} = (x, y)$ in $\mathbf{o}_t$ where the robot will grasp. This point can be converted into a 6 DoF gripper pose by projecting it onto the 3D scene using depth values from the corresponding depth image, and then incorporating known camera parameters [14] for a target position. This does not specify the orientation of the gripper, but since the position of the bed frame is known, the gripper rotates to be orthogonal to the bed.

Let the *transition policy* be $\pi_{\theta_T} : \mathbb{R}^{640\times480\times3} \rightarrow \{0, 1\}$ parameterized by θ_T, which maps $\mathbf{o}_t$ to a binary decision $\mathbf{u}_t^{(T)} \in \{0, 1\}$ as to whether it should transition to the other side; equivalently, whether the prior grasp succeeded.

The two policies interleave with each other as follows. At the initial side, once the grasp location has been determined, the robot moves its (open) gripper to the location, closes it, and then pulls towards the nearest uncovered corner of the bed. Afterwards, the robot checks whether its action was successful. Due to blanket properties and the stochastic nature of actions, a re-grasp may be necessary. Examples of successful and failed grasps are shown in Figure 3. To decide whether the robot should retry at time t, it queries the transition policy π_{θ_T} and receives a binary signal $\mathbf{u}_t^{(T)}$. Once the robot receives the signal that the blanket is sufficiently stretched on one side, it moves to the other side and repeats.

[1] Assigning corners as grasping points differs from our earlier preprint [20] and has the advantage of accelerating data collection for training policies, since a corner can be automatically labeled with a color marker.

C. Data Collection

We use supervised learning to train π_{θ_G} and π_{θ_T}. The grasp policy needs to detect corners from depth images, which can be difficult to determine analytically due to the deformable nature of blankets. For the transition policy, while one could define it by using a marker on the bed frame and running a test to see whether it is visible or covered, markers will not be available in general. Moreover, a blanket may technically cover a marker but still look unkempt according to a particular human's tastes, motivating the need for a trainable policy.

To collect training data for π_{θ_G}, we use a white blanket with a red corner marker. For sampling the initial state, we keep two blanket ends fixed to the bed and then toss the remaining part onto the bed. We re-toss if the nearest blanket corner is not visible or unreachable from the robot's position, which can be viewed as rejection sampling to find a valid initial state. Figure 4 shows representative initial states, which are substantially more diverse than those in our earlier preprint [20] which was limited to using a single fold.

Given the initial state, we then manually perform short pulls of the blanket and collect a dataset $\mathcal{D}_G = \{(\mathbf{o}_i, \mathbf{u}_i^{(G)})\}_{i=1}^N$ for training the grasp policy, occasionally re-tossing the blanket as needed. Labels $\mathbf{u}_i^{(G)}$ correspond to pixels of the red marked corner location in $\mathbf{o}_i$ and are automatically annotated from the RGB images. While performing bed-making demonstrations, we simultaneously obtain a smaller dataset $\mathcal{D}_T = \{(\mathbf{o}_i, \mathbf{u}_i^{(T)})\}_{i=1}^M$ for training the transition policy, which requires manual human labeling for the binary outcomes $\mathbf{u}_i^{(T)}$. This process resulted in 2018 and 654 data points for training the respective grasp and transition policies.

D. Training Neural Network Policies

We parameterize π_{θ_G} and π_{θ_T} with separate deep convolutional neural networks. As in our earlier work [20], for both policies we use an architecture based on YOLO [34], a popular real-time object detection network. An advantage of using YOLO is speed; it is fast compared to other object detection methods, which is ideal for real-time control tasks.

We utilize pre-trained weights optimized on Pascal VOC 2012 [8]. This is due to the potential for transfer learning [38] since the task of detecting a grasp point has similarities with detecting a bounding box in 2D space and providing a classification label. We call this network *YOLO Pre-Trained*; see Figure 5 for an overview. We fix the first 32 million parameters from YOLO and optimize two additional convolutional layers and two dense layers. We also apply data augmentation techniques, such as a flip about the vertical axis to simulate being on the opposite side of the bed, to get 10x more training data. The parameters of π_{θ_G} and π_{θ_T} are

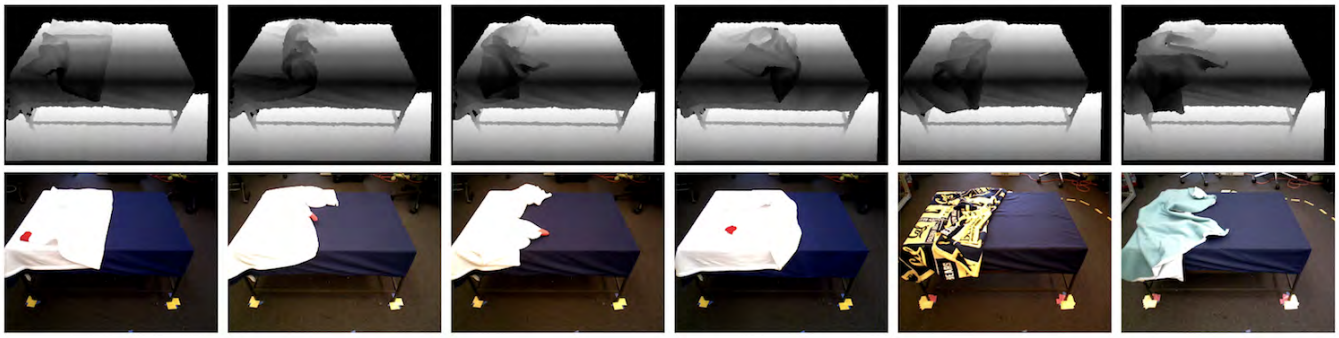

Fig. 4: Examples of initial states. The grasp and transition policies are trained with depth images (top row, with corresponding RGB images below). The grasp network training data is automatically labeled with the red marker from the RGB image. To avoid background noise, we black out regions beyond a validation-tuned depth value. During testing, we use the same white blanket along with a Cal and a teal blanket (see Section V). The initial states are substantially more diverse than those in our earlier preprint [20]; see the supplementary material for additional examples.

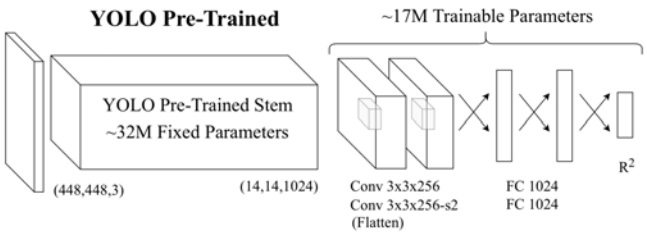

Fig. 5: The network architecture we used for grasping and transitioning. From a $(448 \times 448 \times 3)$-sized input image, we use pre-trained weights to obtain a $(14 \times 14 \times 1024)$-sized tensor. Then, we optimize two convolutional and two dense layers, resulting in about 17 million adjustable parameters. Notation: "s" indicates stride, and two crossing arrows are a dense layer.

optimized via Adam [17] by minimizing the L_2 and binary cross-entropy losses, respectively.

Since YOLO Pre-Trained uses weights that were trained on RGB images and our task uses *depth* images, we additionally tested full training of YOLO without fixing the first 32 million parameters, but found this to lead to worse performance with more than double the L_2 pixel error. Full training details and comparisons with alternative training protocols and architectures are in the supplementary material.

V. Experiments and Policies

We perform experiments to test: 1) neural network architectures and training procedures, 2) robustness of the learned policies to different robots and different blankets, and 3) comparisons of learning versus an analytic baseline.

A. Neural Network Training Results

We trained the grasp and transition networks over data from Section IV-C, with hyperparameters determined via 10-fold cross validation. Figure 6 demonstrates training results of the grasping network over the best hyperparameter set. It shows the L_2 pixel prediction losses (over each data point when it was in a validation set fold) as a function of training epoch, showing that it converges to roughly 27.4 pixel error.

Figure 6 also presents a scatter plot of the the distribution of training points (i.e., blanket corners) and a heat map of those points and their held-out L_2 losses (again, in pixels) for the best-performing validation set iteration. As expected, the heat map generally shows darker regions towards the extremes of the dataset, particularly to the left and bottom. These correspond to when blanket corners are far away from the frame target or close to the edge of the top surface.

Transition Network	0.5 Ep.	1 Ep.	5 Ep.	10 Ep.
YOLO Pre-Trained	635/654	643/654	645/654	648/654

TABLE I: Classification accuracy of the transition network as a function of training epoch (over augmented data). We used 654 real images, and performance is based on the sum of 10 cross validation folds.

Table I shows results for the transition network. When trained on 654 data points with an equal distribution of successful and failure cases, YOLO Pre-Trained quickly achieves near-perfect performance to about 648/654 correct. Incorrectly classified images tend to be "borderline" cases which could reasonably be considered either a success or failure. When deployed in a home, such a network could be tuned to a particular human's preferences.

B. Baseline Policies: Human, Highest-Point and RGB

We compare our proposed method using YOLO Pre-Trained with two grasp policies: a human selecting grasp points via a click interface and an analytic baseline where the robot grips the highest reachable point $(x, y, f_\xi(x, y)) \in E_\xi$ of the bed. These comparisons help us in characterizing the difficulty of our setup, in quantifying the improvement of using Deep Learning as opposed to analytic policies, and in seeing how close a trained policy can match a human supervisor.

The analytic policy is a strong baseline. The highest point can correspond to a corner fold, in which case the policy will do well since grasping near corners almost always results in excellent coverage. Even if the highest point is not the corner, blankets can stretch (e.g., Figure 7) and the pull flattens the nearby region of the blanket and may make the subsequent highest point closer to the blanket corner.

For testing transfer to Cal and teal blankets (see Figure 8), we also benchmark our depth-based policy with a policy trained on RGB images of the white blanket. Other than the training data change, this RGB-policy was trained in an identical manner as the depth policy.

C. Policy Evaluation Procedure

We test the depth-based neural network, human, and highest-point grasp policies on the same white blanket from training using the HSR and the Fetch. In addition, we use the HSR to test transfer learning to different blankets and compare with the RGB-based policy.

We report average coverage per rollout, which involves grasping and pulling at the two longer sides of the bed. Before

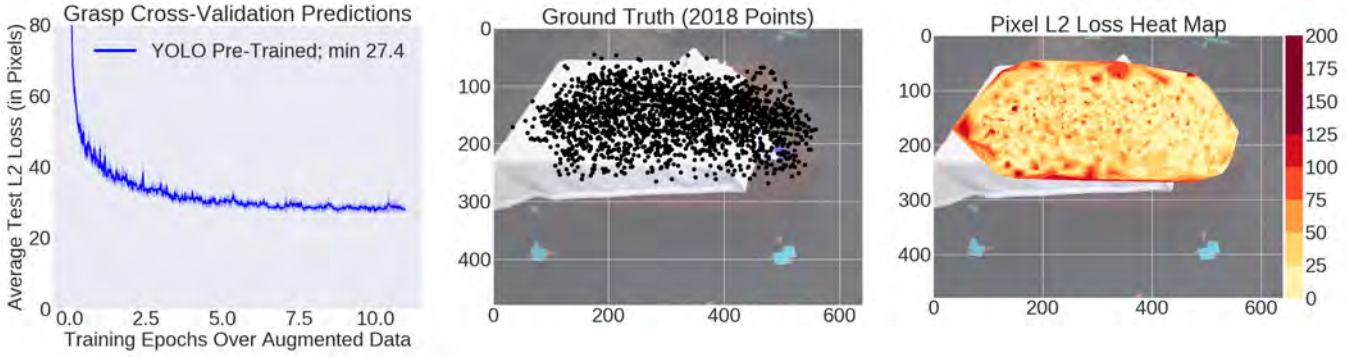

Fig. 6: Left: validation set L_2 errors (in pixels) when training the grasp policy on depth data. The curve is averaged over 10-fold cross validation runs, with one standard deviation shaded. Middle: a scatter plot showing the distribution of corners (i.e., grasp points) in our combined data of 2018 images. Right: heat map performance of YOLO Pre-Trained on the data, where each of the 2018 points was part of a validation test due to 10-fold cross validation. We report results for the best validation-set performance for each of the 10 models. The heat map is based on L_2 error in pixel space. Both subplots are overlaid on top of an image of the bed that has a similar viewpoint as to what the robot would see during rollouts.

Fig. 7: The analytic baseline can often do reasonably well because the white blanket is smooth and stretchy. While the initial pull above achieves reasonable coverage, it covers a blanket corner and makes it harder for subsequent grasps and pulls to make nontrivial coverage progress.

Fig. 8: Three blankets we use for evaluation. Left: white, used for data collection with a red corner. Center: Cal, with non-homogeneous patterns. Right: teal, with a thin white blanket pinned underneath it.

each rollout, we toss a blanket for the initial state and *then* randomly choose the policy to use, to avoid human bias in making easier setups for the depth-based neural network policy. In addition, for all experiments, we use the same transition neural network policy π_{θ_T} for consistency. Finally, we allow up to four grasp and pull attempts per side.

For evaluating blanket coverage, we measure the area of the top of the bed frame and the area of its uncovered portion using a top-down camera image.

VI. Bed-Making Results

A. Coverage

For each experimental condition, we execute between 12 and 24 rollouts with different initial blanket setups. Figure 9 shows exact rollout counts, along with average initial and final coverage results.[2]

The results suggest that the neural network policy on the white blanket, which attains 93.2 ± 6.6 and 89.8 ± 9.1 percent coverage for the HSR and Fetch, respectively, outperforms the analytic baseline which achieves 84.6 ± 7.7 and 80.5 ± 14.7 coverage. We ran a Mann-Whitney U test [25] to compare coverage on the white blanket among the analytic and learned policies for the HSR (24 rollouts each), and obtained a p-value of $p = 0.00034$, strongly suggesting statistically significant differences. See the supplementary material for more details.

The trained grasp policy is nearly as good as the human supervisor which gets 96.4 ± 4.3 and 92.8 ± 10.2. These results are consistent among the two robots, providing evidence of the robot-to-robot transfer capability of our method.[3]

For transfer to Cal and teal blankets, the HSR gets 91.7 ± 5.3 and 93.3 ± 5.0 coverage, respectively. These results indicate that a neural network grasp policy trained on depth images (of the white blanket) directly transfers to two other blankets despite slightly different material properties; the Cal blanket is thinner, while the teal blanket does not stretch as much and has a thin white sheet pinned underneath it.

From Figure 9, we also observe that the RGB-based policy (for the HSR) only obtains 85.5 ± 8.1 and 86.2 ± 8.4 percent coverage on the Cal and teal blankets, showcasing the limits of RGB-based transfer. Empirically, we observe that the RGB-based policy consistently grasps the Cal blanket close to its center. For the Teal blanket, it tends to grasp anywhere along the exposed white underside, or near the center if there is no white visible. These are inferior policies as compared to grasping at corners.

B. Policy Visualization

Figure 10 shows example RGB images from the robot's sensors in one rollout when it was using the depth-based policy (i.e., it only used depth for decision-making) with the teal blanket. The initial prediction was correctly near a corner, but the robot was unable to pull the blanket all the way to the frame corner due to friction and a "weak" grip which had an offset that was slightly too high and thus barely held the corner. This resulted in the blanket corner off to the side, as shown in the top right image.

When this happens, our learned policy tends to predict points close to the blanket corner but which are on top of the bed. This is a reasonable policy and allows the robot to

[2]We use initial coverage to understand relative coverage gain, but it is not a perfect metric of task difficulty because a blanket can cover the majority of the frame but have corners in difficult-to-reach locations.

[3]When pooling together HSR and Fetch results, we get 91.7% and 95.0% coverage for the learned policy and human supervisors, which are the values reported in the abstract and in Section I.

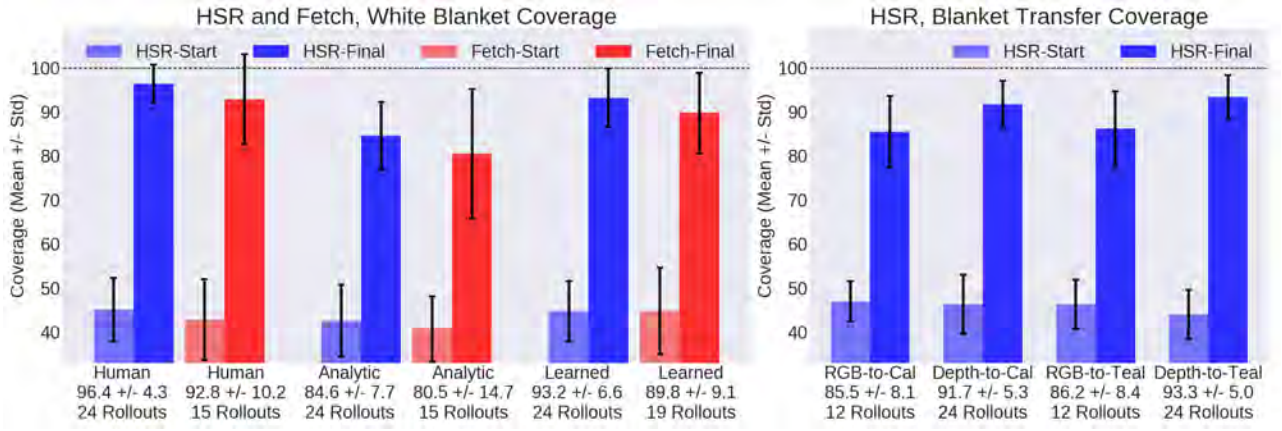

Fig. 9: Initial and final coverage results, grouped together, under setups as outlined in Sections V-B and VI-A. **Left**: results with the HSR (blue) and Fetch (red) for the white blanket. *Human*: human selecting grasp points. *Analytic*: the highest reachable point policy. *Learned*: depth-based (from white blanket) neural network grasp policy. **Right**: HSR-only coverage results testing blanket transfer. *RGB-to-Cal* and *RGB-to-Teal*: the RGB-based grasp policy on Cal and teal blankets. *Depth-to-Cal* and *Depth-to-Teal*: depth-based neural network grasp policy (same as in *Learned*) on Cal and teal blankets. Bars report averages and one sample standard deviation across the number of rollouts listed in the x-axis labels, which also reports the final coverage.

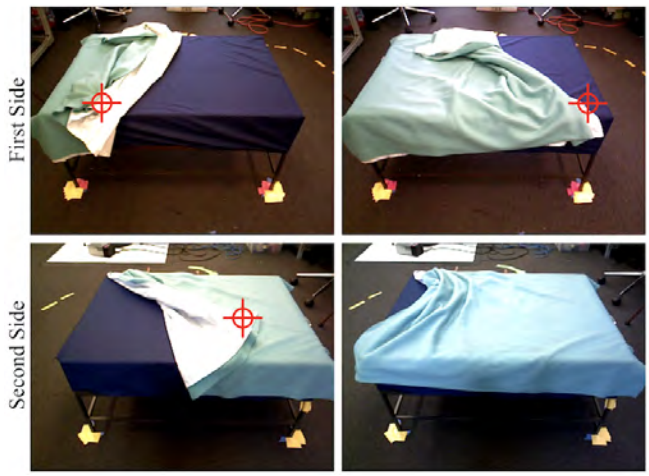

Fig. 10: Examples of images from the robot's sensors as it executes the trained grasp (and transition) policies; we use RGB for clarity but the robot only used depth images in this rollout. Predictions from the grasp network are shown with a red cross hair. Top row: initially, the robot correctly picks a corner but doesn't manage to pull the blanket all the way due to friction, and the corner is not on the top of the bed. The robot makes incremental coverage progress in the subsequent grasp attempt. Bottom row: on the second side, it correctly predicts the corner and only needs one grasp and pull attempt.

make incremental coverage in future attempts. On the other side, the policy also predicted near a corner, but the robot was able to grip it firmly and did not need additional grasp attempts.

C. Length and Timing

With up to four grasp attempts each side, there are a maximum of eight attempts per rollout. On the white blanket rollouts, the highest-point baseline required an average of 6.2 and 4.9 grasp attempts for the HSR and Fetch, respectively, compared to 4.4 and 4.3 for the learned policy, and 2.8 and 3.0 for the human supervisor. The baseline took longer because it often covered the blanket corner during the first pull and did not achieve sufficient coverage (e.g., as in Figure 7). Thus, the learned transition policy would tell the robot to re-attempt a grasp and pull, yet the subsequent grasps made minimal coverage progress.

We performed experiments on a single workstation with an NVIDIA Titan Xp GPU, and timed three major components of each rollout: moving to another side of the bed, physical grasp execution, and neural network forward passes. These required an average of 32.1, 17.7, and 0.1 seconds for the HSR, and 28.9, 87.9, and 0.1 seconds for the Fetch, showing that movement and grasping speed are the main time bottlenecks.

D. Limitations With Corners

We assume blanket corners are visible and on the top surface in the initial state. This assumption may get violated in subsequent states. For example, in Figure 7 the robot pulled the blanket over the corner, and in Figure 10 the corner is off to the side in the top right image. When these cases occur, as mentioned in Section VI-B, the grasp network typically picks a point somewhere along the edge of the blanket on top of the bed frame, such as in the top right subplot of Figure 10.

This can make incremental coverage in some cases, but if the top envelope E_ξ of the blanket near the blanket corner region is relatively smooth, such as in Figure 7, the grasping policy will normally be unable to make further coverage progress on that side of the bed.

VII. Conclusions and Future Work

This paper uses supervised learning to teach mobile robots to make a bed across multiple blanket configurations and colors. There are a number of future work directions, such as extending the method for application to furniture covers, table cloths, and other deformable objects commonly seen in homes. An additional extension is to develop policies that can pull out and reveal hidden or unreachable corners.

Acknowledgments

This research was performed at the AUTOLAB at UC Berkeley in affiliation with the Berkeley AI Research (BAIR) Lab, Berkeley Deep Drive (BDD), the Real-Time Intelligent Secure Execution (RISE) Lab, and the CITRIS "People and Robots" (CPAR) Initiative, and by the Scalable Collaborative Human-Robot Learning (SCHooL) Project, NSF National Robotics Initiative Award 1734633. The authors were supported in part by donations from Siemens, Google, Amazon Robotics, Toyota Research Institute, Autodesk, ABB, Samsung, Knapp, Loccioni, Honda Research Institute USA, Intel, Comcast, Cisco, Hewlett-Packard and by equipment grants from PhotoNeo, NVidia, and Intuitive Surgical. We thank our colleagues who provided helpful feedback and suggestions, in particular Ashwin Balakrishna, Carolyn Chen, David Chan, Zisu Dong, Roshan Rao, and Brijen Thananjeyan; we are also deeply indebted to TMC and TRI for their assistance with the HSR on short notice. Daniel Seita is supported by a National Physical Science Consortium Fellowship.

REFERENCES

[1] B. D. Argall, S. Chernova, M. Veloso, and B. Browning, "A survey of robot learning from demonstration," *Robotics and autonomous systems*, vol. 57, no. 5, pp. 469–483, 2009.

[2] B. Balaguer and S. Carpin, "Combining Imitation and Reinforcement Learning to Fold Deformable Planar Objects," in *IEEE/RSJ International Conference on Intelligent Robots and Systems (IROS)*, 2011.

[3] J. M. Beer, C.-A. Smarr, T. L. Chen, A. Prakash, T. L. Mitzner, C. C. Kemp, and W. A. Rogers, "The Domesticated Robot: Design Guidelines for Assisting Older Adults to Age in Place," in *ACM/IEEE International Conference on Human-Robot Interaction (HRI)*, 2012.

[4] J. Bloomfield, A. Pegram, and A. Jones, "Recommended Procedure for Bedmaking in Hospital," *Nursing Standard*, vol. 22, 2008.

[5] M. C. Clark, S. J. Czaja, and R. A. Weber, "Older Adults and Daily Living Task Profiles," *Human Factors*, vol. 32, no. 5, 1990.

[6] M. Cusumano-Towner, A. Singh, S. Miller, J. F. O'Brien, and P. Abbeel, "Bringing Clothing Into Desired Configurations with Limited Perception," in *IEEE International Conference on Robotics and Automation (ICRA)*, 2011.

[7] Z. Erickson, H. M. Clever, G. Turk, C. K. Liu, and C. C. Kemp, "Deep Haptic Model Predictive Control for Robot-Assisted Dressing," in *IEEE International Conference on Robotics and Automation (ICRA)*, 2018.

[8] M. Everingham, L. Van Gool, C. K. I. Williams, J. Winn, and A. Zisserman, "The PASCAL Visual Object Classes Challenge 2012 (VOC2012) Results," http://www.pascal-network.org/challenges/VOC/voc2012/workshop/index.html.

[9] N. Ezer, A. Fisk, and W. Rogers, "More than a Servant: Self-Reported Willingness of Younger and Older Adults to having a Robot perform Interactive and Critical Tasks in the Home," *Proc Hum Factors Ergon Soc Annu Meet*, 2009.

[10] C. B. Fausset, A. J. Kelly, W. A. Rogers, and A. D. Fisk, "Challenges to Aging in Place: Understanding Home Maintenance Difficulties," *Journal of Housing for the Elderly*, vol. 25, no. 2, pp. 125–141, 2011.

[11] I. Goodfellow, Y. Bengio, and A. Courville, *Deep Learning*. MIT Press, 2016, http://www.deeplearningbook.org.

[12] A. Gupta, A. Murali, D. Gandhi, and L. Pinto, "Robot Learning in Homes: Improving Generalization and Reducing Dataset Bias," in *Neural Information Processing Systems (NIPS)*, 2018.

[13] K. Hashimoto, F. Saito, T. Yamamoto, and K. Ikeda, "A Field Study of the Human Support Robot in the Home Environment," in *IEEE Workshop on Advanced Robotics and its Social Impacts*, 2013.

[14] B. Horn, *Robot Vision*. MIT Press, 1986.

[15] S. Khadka, D. Kisi, P. Raya, and S. Shrestha, "Fundamentals of Nursing Procedures for PCL Course," *Japan International Cooperation Agency (JICA) Nepal Office*, 2008.

[16] C.-H. King, T. L. Chen, A. Jain, and C. C. Kemp, "Towards an Assistive Robot that Autonomously Performs Bed Baths for Patient Hygiene," in *IEEE/RSJ International Conference on Intelligent Robots and Systems (IROS)*, 2010.

[17] D. P. Kingma and J. Ba, "Adam: A Method for Stochastic Optimization," in *International Conference on Learning Representations (ICLR)*, 2015.

[18] A. Krizhevsky, I. Sutskever, and G. E. Hinton, "ImageNet Classification with Deep Convolutional Neural Networks," in *Neural Information Processing Systems (NIPS)*, 2012.

[19] M. Laskey, J. Lee, R. Fox, A. Dragan, and K. Goldberg, "DART: Noise Injection for Robust Imitation Learning," in *Conference on Robot Learning (CoRL)*, 2017.

[20] M. Laskey, C. Powers, R. Joshi, A. Poursohi, and K. Goldberg, "Learning Robust Bed Making using Deep Imitation Learning with DART," *arXiv:1711.02525*, 2017.

[21] A. X. Lee, H. Lu, A. Gupta, S. Levine, and P. Abbeel, "Learning Force-Based Manipulation of Deformable Objects From Multiple Demonstrations," in *IEEE International Conference on Robotics and Automation (ICRA)*, 2015.

[22] K. M. Lynch and F. C. Park, *Modern Robotics: Mechanics, Planning, and Control*. Cambridge University Press, 2017.

[23] J. Mahler, J. Liang, S. Niyaz, M. Laskey, R. Doan, X. Liu, J. A. Ojea, and K. Goldberg, "Dex-Net 2.0: Deep Learning to Plan Robust Grasps with Synthetic Point Clouds and Analytic Grasp Metrics," in *Robotics: Science and Systems (RSS)*, 2017.

[24] J. Maitin-Shepard, M. Cusumano-Towner, J. Lei, and P. Abbeel, "Cloth Grasp Point Detection Based on Multiple-View Geometric Cues with Application to Robotic Towel Folding," in *IEEE International Conference on Robotics and Automation (ICRA)*, 2010.

[25] H. B. Mann and D. R. Whitney, "On a Test of Whether one of Two Random Variables is Stochastically Larger than the Other," *The Annals of Mathematical Statistics*, 1947.

[26] J. Matas, S. James, and A. J. Davison, "Sim-to-Real Reinforcement Learning for Deformable Object Manipulation," *arXiv:1806.07851*, 2018.

[27] S. Miller, J. van den Berg, M. Fritz, T. Darrell, K. Goldberg, and P. Abbeel, "A Geometric Approach to Robotic Laundry Folding," in *International Journal of Robotics Research*, 2012.

[28] T. Mukai, S. Hirano, H. Nakashima, Y. Kato, Y. Sakaida, S. Guo, and S. Hosoe, "Development of a Nursing-Care Assistant Robot RIBA That Can Lift a Human in Its Arms," in *IEEE/RSJ International Conference on Intelligent Robots and Systems (IROS)*, 2010.

[29] A. Murali, S. Sen, B. Kehoe, A. Garg, S. McFarland, S. Patil, W. D. Boyd, S. Lim, P. Abbeel, and K. Goldberg, "Learning by Observation for Surgical Subtasks: Multilateral Cutting of 3D Viscoelastic and 2D Orthotropic Tissue Phantoms," in *IEEE International Conference on Robotics and Automation (ICRA)*, 2015.

[30] Ohea, "Ohea - The Smart Bed," http://www.ohea.eu/.

[31] D. Park, H. Kim, Y. Hoshi, Z. Erickson, A. Kapusta, and C. C. Kemp, "A Multimodal Execution Monitor with Anomaly Classification for Robot-Assisted Feeding," in *IEEE/RSJ International Conference on Intelligent Robots and Systems (IROS)*, 2017.

[32] G. C. Pellatt, "Clinical Skills: Bed Making and Patient Positioning," *British Journal of Nursing*, 2007.

[33] D. A. Pomerleau, "Alvinn: An Autonomous Land Vehicle in a Neural Network," Carnegie-Mellon University, Tech. Rep., 1989.

[34] J. Redmon, S. Divvala, R. Girshick, and A. Farhadi, "You Only Look Once: Unified, Real-Time Object Detection," in *IEEE Conference on Computer Vision and Pattern Recognition (CVPR)*, 2016.

[35] S. Ross, N. Melik-Barkhudarov, K. S. Shankar, A. Wendel, D. Dey, J. A. Bagnell, and M. Hebert, "Learning Monocular Reactive UAV Control in Cluttered Natural Environments," in *IEEE International Conference on Robotics and Automation (ICRA)*, 2013.

[36] J. Schulman, A. X. Lee, J. Ho, and P. Abbeel, "Tracking Deformable Objects with Point Clouds," in *IEEE International Conference on Robotics and Automation (ICRA)*, 2013.

[37] K.-H. Seo, C. Oh, T.-Y. Choi, and J.-J. Lee, "Bed-Type Robotic System for the Bedridden," in *IEEE International Conference on Advanced Intelligent Mechatronics*, 2005.

[38] A. Sharif Razavian, H. Azizpour, J. Sullivan, and S. Carlsson, "CNN Features Off-the-Shelf: An Astounding Baseline for Recognition," in *IEEE Conference on Computer Vision and Pattern Recognition, workshop*, 2014.

[39] S. Shibata, T. Yoshimi, M. Mizukawa, and Y. Ando, "A Trajectory Generation of Cloth Object Folding Motion Toward Realization of Housekeeping Robot," in *International Conference on Ubiquitous Robots and Ambient Intelligence (URAI)*, 2012.

[40] B. Thananjeyan, A. Garg, S. Krishnan, C. Chen, L. Miller, and K. Goldberg, "Multilateral Surgical Pattern Cutting in 2D Orthotropic Gauze with Deep Reinforcement Learning Policies for Tensioning," in *IEEE International Conference on Robotics and Automation (ICRA)*, 2017.

[41] H.-C. Wang, R. K. Katzschmann, S. Teng, B. Araki, L. Giarre, and D. Rus, "Enabling Independent Navigation for Visually Impaired People through a Wearable Vision-Based Feedback System," in *IEEE International Conference on Robotics and Automation (ICRA)*, 2017.

[42] M. Wise, M. Ferguson, D. King, E. Diehr, and D. Dymesich, "Fetch & Freight: Standard Platforms for Service Robot Applications," in *IJCAI Workshop on Autonomous Mobile Service Robots*, 2016.

[43] W. Yu, A. Kapusta, J. Tan, C. C. Kemp, G. Turk, and C. K. Liu, "Haptic Simulation for Robot-Assisted Dressing," in *IEEE International Conference on Robotics and Automation (ICRA)*, 2017.

[44] T. Zhang, Z. McCarthy, O. Jow, D. Lee, X. Chen, K. Goldberg, and P. Abbeel, "Deep Imitation Learning for Complex Manipulation Tasks from Virtual Reality Teleoperation," in *IEEE International Conference on Robotics and Automation (ICRA)*, 2018.

APPENDIX I
BED-MAKING AS AN MDP

The bed-making problem can be formalized as an MDP $\mathcal{M} = \langle \Xi, \mathcal{A}, P, \rho_0, R, \gamma \rangle$ where

1) Ξ is the set of possible states, where state $\xi_t \in \Xi$ is the blanket configuration at time t.
2) $\mathcal{A}$ is the set of possible actions, where each action $a_t \in \mathcal{A}$ is a tuple $a_t = (\mathbf{u}_t^{(T)}, \mathbf{u}_t^{(G)})$ which consists of the binary signal $\mathbf{u}_t^{(T)} \in \{0, 1\}$ indicating whether the robot should move to the other side of the bed, and the 2D grasp point $\mathbf{u}_t^{(G)} \in \mathbb{R}^2$ as subsequently viewed through the robot's cameras.
3) $P : \Xi \times \mathcal{A} \times \Xi \to \mathbb{R}$ is the transition probability distribution (not to be confused with the transition *network* policy π_{θ_T}) in which $p(\xi_{t+1}|\xi_t, a_t)$ gives the next state given that the robot was at ξ_t and took action a_t. This is difficult to accurately model due to specifying the next blanket configuration.
4) $R : \Xi \times \mathcal{A} \times \Xi \to \mathbb{R}$ is the reward function (e.g., see Equation 4) where $R(\xi_t, a_t, \xi_{t+1})$ gives the reward obtained after the robot, at state ξ_t, executes action a_t and lands in ξ_{t+1}.
5) ρ_0 is the initial state distribution, which gives the probability of $\xi_0 \in \Xi$ being drawn.
6) $\gamma \in [0, 1]$ is the discount factor.

The states are Markovian because we assume a sufficient time interval to make the blanket stationary after each grasp and pull, so there is no "momentum" from prior actions. Our proposed solution (described in Section IV) uses grasp π_{θ_G} and transition π_{θ_T} networks, which is compatible with the action formulation since it implicitly encodes moving to another side as needed. In the formulation here, the movement comes first in the action tuple since the blanket state does not change in the process of the robot transitioning, whereas it (almost always) changes after a grasp and pull attempt.

We assume that the agent can position itself on one side to get a sufficiently expressive view of the frame and blanket. Technically, some parts of the blanket state ξ_t are not visible (e.g., material that folds underneath another layer) and the robot must make its decisions based on the *observation* $\mathbf{o}_t$. The information that is hidden from $\mathbf{o}_t$, though, is not relevant for determining the rewards R and transition model P. Therefore, even though the robot cannot specify every detail of the blanket, the bed-making setup is still an MDP and not a POMDP.

One can attempt to construct a reward function that would roughly reflect our procedure of grasping and transitioning. As a start, given current coverage $c(\xi_t)$ at time t (where $c(\xi_t) \in [0, 1]$), we can measure the reward of taking action a_t by relative coverage gain $c(\xi_{t+1}) - c(\xi_t)$. This would take into account that we want the robot to efficiently pull a blanket to one corner before moving to another (in as few grasp and pull attempts as possible).

One issue that arises, though, is if higher relative coverage gain can be attained by moving to the other side of the bed before the current side has been sufficiently stretched. Hence, we can add a negative reward function T if the agent has to transition to another side,

$$T(a_t; \lambda_1) = T\Big((\mathbf{u}_t^{(T)}, \mathbf{u}_t^{(G)}); \lambda_1\Big) = \lambda_1 \cdot \mathbb{I}\Big(\mathbf{u}_t^{(T)}\Big), \quad (3)$$

where $\mathbb{I}$ is an indicator function equal to one if the value inside is one (and zero otherwise) and $\lambda_1 < 0$ is a constant. This would remove the incentive to go back and forth across sides to obtain larger relative rewards, though the reward cannot be so negative that the agent never has an incentive to transition to the other side to get higher coverage. Hence, we can have

$$R(\xi_t, a_t, \xi_{t+1}) = (c(\xi_{t+1}) - c(\xi_t)) + T(a_t; \lambda_1) \quad (4)$$

for $c(\xi_t) \in [0, 1]$ and an appropriate value of $\lambda_1 < 0$.

APPENDIX II
TRAINING DETAILS

For training grasp policies π_{θ_G}, all observations $\mathbf{o}_t \in \mathbb{R}^{640 \times 480 \times 3}$ are scaled to be $(448, 448, 3)$ and then passed to the YOLO Pre-Trained network. We additionally scale the grasp labels to be in the range of $[-1, 1]$, to better condition the optimization.

We tried dropout and/or batch normalization on the last fully connected layer, but found this to be no better than training without it. Hence, we do not use either regularization technique. We use Adam for optimization; as an alternative, we tried Stochastic Gradient Descent with an exponential moving average for weight updates, but found that to lead to consistently worse performance. Full hyperparameter details for our final model are in Table II.

Hyperparameter	**Value**
L_2 Regularization	0.0001
Adam Learning Rate	0.0001
Batch Size	64
Training Epochs	12
Leaky ReLU α	0.1

TABLE II: Hyperparameters used for the final trained *grasp* networks, based on YOLO Pre-Trained. The transition network used the same hyperparameters as listed here, except with 16 training epochs (its dataset is smaller).

The grasp and transition networks were benchmarked via 10-fold cross validation to find when the training loss reached rough convergence, and then the training was re-done for a similar number of steps but with all the folds used in the training data.

During training, we apply extensive data augmentation techniques. We double our dataset by reflecting the image around the vertical axis. Intuitively, this transformation helps because a vertical flip creates an image that has the perspective similar to the opposite side of the bed. For depth images, we also apply changes by:

- adding uniform noise
- adding Gaussian noise
- adding black dots randomly
- adding black and white dots randomly

These techniques result in a 10x larger training set.

APPENDIX III
ADDITIONAL TRAINING EXPERIMENTS

In addition to YOLO Pre-Trained, we test with the same YOLO-based architecture, but without fixing the first 32

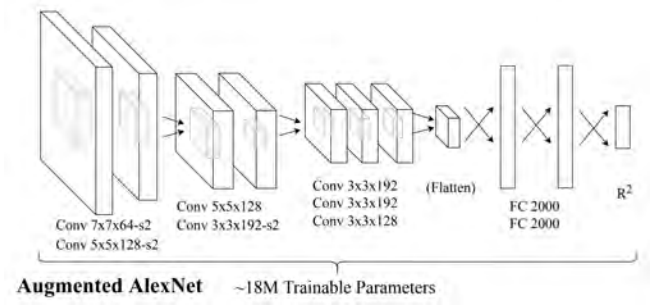

Fig. 11: An alternative neural network architecture we tested, called *Augmented AlexNet*. We use three groups of convolutional and max-pooling layers. Two dense layers conclude the network, which has about 18 million parameters. *Notation*: converging arrows are 2x2 max-pooling layers, crossing arrows are dense layers, and "s2" means a stride of 2, with stride 1 as the default.

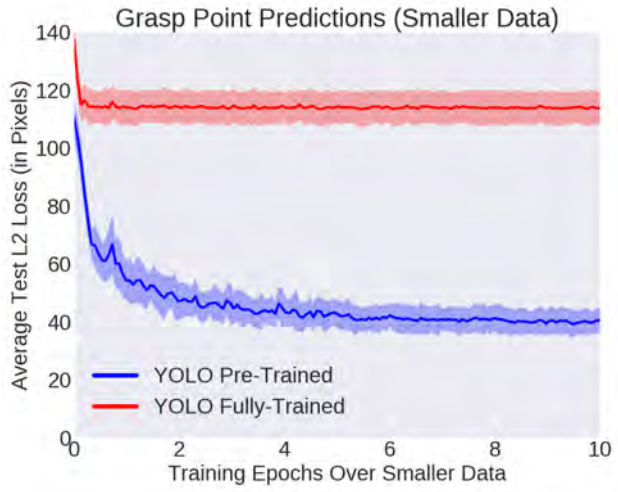

Fig. 12: Performance of YOLO Pre-Trained and YOLO Fully-Trained on a subset of the full grasping data we used. Curves are averaged over 10-fold cross validation runs.

million parameters. This is to test if there are limits to transfer learning since the pre-trained weights are from an RGB-based dataset, and our task uses depth images. In this network, which we call *YOLO Fully-Trained*, we initialize the weights using the same pre-trained weights and follow the same hyperparameters as YOLO Pre-Trained.

Due to the high computational and memory requirements of training YOLO Fully-Trained, we test the two training protocols on a subset which is 25% of the size of our full data of 2018 grasp points. The loss curves from 10-fold cross validation, shown in Figure 12, strongly suggest that YOLO Pre-Trained is better for our task, since YOLO Fully-Trained struggles to get below 120 pixels in L_2 error.

We additionally test a second network architecture based on a variation of AlexNet [18] where we add several more convolutional layers between the pooling layers, but use a smaller number of layers compared to YOLO. We test this architecture in case the large number of layers and parameters (including the pre-trained portion) was causing YOLO Pre-Trained to overfit, and in case it would be better for the *transition* network, which does not involve detection. We call this alternative network *Augmented AlexNet*; see Figure 11 for an overview. It contains a comparable amount of *trainable* parameters as YOLO Pre-Trained.

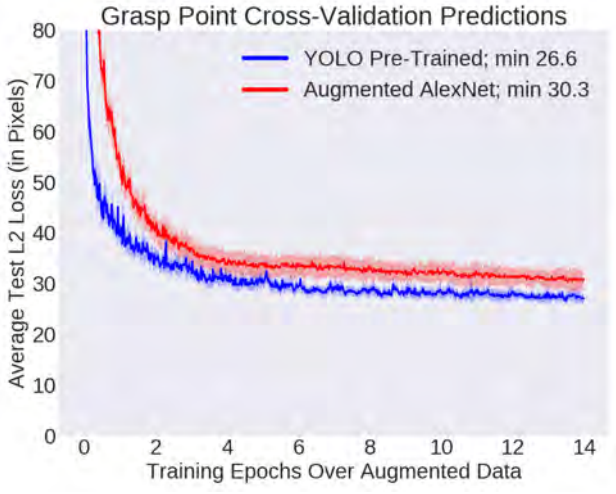

Fig. 13: Performance of neural network grasp policies, measured in terms of L_2 pixel error on validation sets for our full grasp dataset of 2018 data points. Results compare YOLO Pre-Trained with Augmented AlexNet. Curves are averaged over all 10 cross-validation folds. The results show a clear benefit to using pre-trained features versus end-to-end training of Augmented AlexNet. Results are also consistent across different folds.

Transition Network	**0.5 Ep.**	**1 Ep.**	**5 Ep.**	**10 Ep.**
YOLO Pre-Trained	635/654	643/654	645/654	648/654
Augmented AlexNet	607/654	612/654	613/654	632/654

TABLE III: Performance of the Augmented Alex-Net transition network as a function of training epoch (over augmented data). The evaluation setup is identical to that of Table I.

Figure 13 reports training results on our full grasping data of 2018 points. The results indicate a clear benefit to utilizing pre-trained weights, as Augmented AlexNet is consistently worse. Hence, we do not use it for deployment.

Performance of the Augmented AlexNet *transition network* is shown in Table III. Augmented AlexNet requires about 10 epochs to obtain equivalent performance of YOLO Pre-Trained after half an epoch (see Table I), suggesting that using pre-trained features for YOLO is beneficial even when the task is classification (i.e., determining a success versus failure) rather than detection.

Due to these results, we use YOLO Pre-Trained for both the grasp and transition networks for deployment.

APPENDIX IV
DETAILS OF THE GRASP POLICY

In order to make bed making cool again, the grasp policy needs to be carefully designed. Given an image $\mathbf{o}_t$ at time t, the grasp policy π_{θ_G} must select a 2D pixel location $\pi_{\theta_G}(\mathbf{o}_t) = \mathbf{u}_t^{(G)} = (x, y)$ for the robot to grasp the blanket. We can project this point onto the 3D scene by first measuring the depth value, z, from the corresponding depth image. The z is determined via the median value of points in a 10×10 bounding box centered around (x, y). Depth images can have some missing data (i.e., NaN elements) due to noise, so when computing the median, we ignore any such points in the bounding box. The (x, y, z) are then projected onto the scene using known camera parameters to form a 3D target. In addition, since the position of the bed frame is known, we can rotate the gripper to be orthogonal to the bed.

Once the grasp location has been determined, the robot moves its open gripper to the location, closes the gripper, and

Fig. 14: Left: the RGB-based grasping policy selects a grasp point at a spot in the lower left and somewhat far from the actual blanket corner. Right: after grasping and pulling, the RGB-based policy continues to pick points near the lower-center portion of the blanket, which results in no additional coverage for that side. The grasping point determined from the RGB-based policy network is shown with the red cross hair. See Figure 15 for a third-person view of the robot when it executes the grasp at the image to the right.

Fig. 15: A third-person view of the HSR when it attempts to conduct a grasp and pull at the point shown in the second image in Figure 14. This is an example of how a grasp and pull attempt may not increase coverage. From the third-person view, the corner of the Cal blanket is to the top left in both images above, yet the robot is gripping towards the top center of the blanket (left image). The resulting grasp and pull (right image) fails to noticeably move the blanket as that area is already relatively smooth.

then pulls towards the nearest un-covered corner of the bed (i.e., the one on the same side as the robot). After this action, the transition policy — which might be a learned transition policy as we use in the main text — may determine that the blanket has not been sufficiently made at the robot's side. This may happen for a myriad of reasons:

1) *Poor grasp targets*. The grasp location may simply be unsuitable for sufficient coverage, such as if it misses touching the blanket entirely, or if it grips a spot far from its corner.
2) *Force limits*. The robot may experience high force at its gripper during the process of pulling a (closed) gripper towards the bed frame corner. This might happen if, for instance, the robot has to move the gripper through a particularly wrinkled region of the blanket. We hand-tune a force limit and automatically open and release the gripper if the force exceeds the threshold.
3) *Inaccurate gripper offset height*. The robot may occasionally close its gripper at a location slightly too high or too low. To avoid mechanical failures with gripping the hard bed frame, we set the height offset of the gripper so that it favors slightly higher grasps. If the grasp was too high and missed grabbing the blanket, we can often detect this by measuring the similarity in images before and after the grasp attempt,[4] and if the similarity exceeds a threshold, we add an extra offset to move the grasp target closer to the bed.

For these reasons, we allow for multiple grasp and pull attempts per bed side, since subsequent grasps can often improve coverage. We use a maximum of four as that empirically provided a reasonable balance between attaining sufficient coverage without taking an undue amount of time.

APPENDIX V
ADDITIONAL BED-MAKING ROLLOUT RESULTS

A. RGB Policy Observations

The grasping policy trained on RGB images of the white blanket (with the marked corner) has difficulty transferring to other blankets, particularly the Cal blanket which has substantially different color patterns. A typical case in a bed-making rollout is shown in Figure 14, where the RGB-based grasping policy tends to pick points roughly in the lower portion of the blanket, between the fixed corner (of the bed frame) to the lower left and to how far the blanket extends along the frame edge to the un-covered corner. This makes sense since corners are often in that region in the training data images.

A grasp and pull at that target results in some initial coverage. Afterwards, though, the RGB-based policy consistently picks points near the central portion of the edge, which is already flat and and therefore results in negligible additional coverage for that side. (The robot may attain more coverage, though, after it hits the maximum of four attempts on the side and transitions to the other). The depth-based grasping policy generalizes better; if a corner is off to the side, the policy usually picks near the closest blanket point on the edge of the top of the bed, which results in better coverage than points near the blanket center.

Figure 15 shows a third-person view of the setup after the first grasp and pull in Figure 14. The robot keeps grasping at the middle of the bed edge, but since the blanket there is already flat, there is little additional coverage.

[4]We use the L_2 norm and structural similarity metrics.

Component	Mean Time (Sec.)	Quantity
Moving to a Side	32.1 ± 1.5	144
Grasp Execution	17.7 ± 2.2	706
Neural Network Pass	0.1 ± 0.2	982
Moving to a Side	28.9 ± 21.5	49
Grasp Execution	87.9 ± 19.1	201
Neural Network Pass	0.1 ± 0.2	82

TABLE IV: Timing results of bed-making rollouts for the HSR (top three rows) and Fetch (bottom three rows), all in seconds along with standard deviation and the total quantity of data points measured. *Moving to a Side*: moving from one side of the bed to another upon completion, happens twice per trajectory. *Grasp Execution*: the process of the robot moving its end-effector to the workspace and pulling to a target. *Neural Network Pass*: the forward pass through the grasping and success networks.

B. Timing Results

We list timing results (in seconds) in Table IV for three major components of the trajectory. The reported numbers combine all relevant trials from Figure 9. The major bottlenecks of bed-making rollouts are for moving to another side, which required 32.1 and 28.9 seconds for the HSR and Fetch, respectively, and grasp execution, which took 17.7 and 87.9 seconds, respectively. In contrast, due to our fast single-shot CNN, the neural network forward passes took just 0.15 seconds on average.

Trial	Human		Analytic		Learned		RGB-to-Cal		Depth-to-Cal		RGB-to-Teal		Depth-to-Teal	
1	58.5	94.3	50.4	89.6	49.9	95.2	38.0	83.8	63.2	94.8	42.1	81.0	52.3	92.3
2	56.1	93.2	50.1	83.8	53.5	98.0	45.6	89.3	43.9	94.8	39.9	88.0	47.3	95.4
3	46.1	99.2	30.1	68.0	35.7	73.3	50.0	82.8	42.5	96.0	43.1	98.1	34.3	76.4
4	39.2	96.4	31.6	76.8	32.0	97.4	43.9	78.3	51.3	95.3	53.2	74.0	37.1	97.8
5	33.1	98.3	33.4	79.2	39.3	84.1	54.7	79.7	42.0	95.1	42.1	76.5	40.0	95.8
6	30.8	97.0	33.7	74.9	42.5	97.3	43.3	76.0	37.0	85.5	46.0	89.5	41.8	93.0
7	46.7	100.0	41.9	79.9	42.2	81.8	46.9	91.8	51.6	76.9	55.6	82.9	45.7	84.4
8	43.8	94.2	38.0	85.0	44.0	91.5	50.1	91.5	44.5	84.9	54.5	81.6	37.1	92.1
9	51.5	96.5	40.5	84.5	44.5	94.4	48.1	70.9	42.1	96.6	38.4	99.8	48.4	98.2
10	44.7	100.0	41.3	84.4	45.9	99.5	41.4	96.8	47.7	94.3	43.3	80.1	44.6	92.4
11	43.9	98.9	36.5	84.6	42.4	91.7	52.5	87.1	40.6	97.9	46.7	99.2	36.1	97.6
12	54.2	97.4	41.1	96.0	43.2	97.5	49.1	98.1	52.6	95.7	50.9	83.2	56.6	95.7
13	45.9	98.5	45.8	88.7	48.4	99.0			45.4	84.4			46.1	98.1
14	38.5	93.9	56.4	85.8	46.8	92.6			43.6	97.6			48.7	95.4
15	41.9	99.4	33.1	97.2	39.1	99.5			47.8	94.6			41.7	100.0
16	39.4	97.7	40.9	84.7	47.8	98.7			46.8	94.6			40.3	91.7
17	49.9	95.6	52.6	95.8	43.8	90.0			51.4	87.8			45.0	92.9
18	41.7	94.9	34.9	86.3	36.9	96.5			44.6	82.1			46.4	93.3
19	43.9	97.8	59.4	98.7	57.3	89.7			35.7	92.8			51.2	95.0
20	44.7	99.6	44.6	77.6	35.8	99.5			36.0	88.1			46.4	93.9
21	45.7	95.7	52.3	84.0	49.8	83.3			43.9	91.9			45.5	94.7
22	58.7	78.0	34.9	70.5	44.0	99.7			42.0	93.5			34.0	93.5
23	50.2	98.7	49.1	90.4	62.9	92.0			57.0	93.5			44.8	84.8
24	34.3	97.2	49.9	83.8	45.8	93.7			57.6	92.9			45.1	95.8
Mean	45.1	96.4	42.6	84.6	44.7	93.2	47.0	85.5	46.3	91.7	46.3	86.2	44.0	93.3
StdDev	7.3	4.3	8.2	7.7	6.8	6.6	4.6	8.1	6.7	5.3	5.6	8.4	5.6	5.0
StdErr	1.5	0.9	1.7	1.6	1.4	1.4	1.3	2.3	1.4	1.1	1.6	2.4	1.1	1.0

TABLE V: All coverage results involving the HSR, with one trial listed per row. Starting and ending coverage values are paired together. The last rows report the corresponding column's mean, standard deviation, and standard error of the mean. Naming conventions are consistent with those in Figure 9.

Trial	Human		Analytic		Learned	
1	35.9	94.9	42.1	80.9	48.6	90.4
2	32.9	56.6	42.5	76.9	58.6	89.3
3	38.4	92.1	31.3	69.8	48.2	99.2
4	40.2	95.6	45.6	67.3	48.8	77.9
5	52.6	96.8	46.2	59.4	60.1	99.1
6	42.5	99.8	48.8	92.0	39.7	72.8
7	38.7	95.4	30.2	89.5	41.7	98.5
8	31.5	88.9	29.2	72.9	32.5	72.7
9	32.4	88.8	36.4	88.0	52.8	99.3
10	58.7	97.4	34.2	95.8	54.8	95.7
11	59.8	97.0	50.5	82.2	31.9	90.3
12	33.7	99.9	44.9	95.4	27.1	84.6
13	50.9	93.3	33.4	45.8	29.8	90.6
14	50.6	97.0	52.4	100.0	50.4	97.8
15	43.5	99.2	43.3	91.6	31.6	78.5
16					49.5	97.9
17					51.5	92.7
18					49.9	79.2
19					43.2	99.1
Mean	42.8	92.8	40.7	80.5	44.8	89.8
StdDev	9.2	10.2	7.4	14.7	9.8	9.1
StdErr	2.4	2.6	1.9	3.8	2.2	2.1

TABLE VI: All coverage results involving the Fetch, with one trial listed per row. Starting and ending coverage values are paired together. Naming conventions are consistent with those in Figure 9.

C. All Coverage Results

All starting and final coverage values for the rollouts involving the HSR and Fetch are shown in Tables V and VI, respectively. These are the source of results for Figure 9.

We can also pool together results. For instance, combining the human supervisor statistics for the Fetch and HSR results in 95.01% coverage for human supervisors, whereas combining the network policies on the white blanket results in 91.67% coverage for learned policies.

To obtain coverage results, we first collected starting and final images of the setup from a top-down webcam for each rollout. Then, we had a human click on the boundary points for the bed and then trace out the appropriate contours. All images we used for coverage can be found on the project website.[5]

To test for statistical significance among different experimental conditions, we use a Mann-Whitney U test. We did not use standard t-tests because our metric, coverage, is not normally distributed.

For the HSR, the Mann-Whitney U test for the analytic versus learned policies (for the white blanket) is $p = 0.00034$, a strong indicator of statistical significance. The same test for the learned policy versus a *human* results in a higher value of $p = 0.0889$, suggesting that the learned policy's performance more closely matches the human supervisor than the analytic baseline. Additional Mann-Whitney U tests for the learned policy on white versus Cal, white versus teal, and teal vs Cal blankets are $p = 0.227$, $p = 0.844$, and 0.327, respectively. These relatively high p-values mean we cannot reject a hypothesis that the coverage samples in each group are from the same distribution. All these comparisons involved 24 rollouts in both categories. We did not run Mann-Whitney U tests for the Fetch setups since the number of data points is smaller.

[5] https://sites.google.com/view/bed-make